

Received November 28, 2021, accepted December 16, 2021, date of publication December 23, 2021, date of current version January 6, 2022.

Digital Object Identifier 10.1109/ACCESS.2021.3138021

# ScarNet: Development and Validation of a Novel Deep CNN Model for Acne Scar Classification With a New Dataset

MASUM SHAH JUNAYED<sup>1,2</sup>, (Member, IEEE), MD BAHARUL ISLAM<sup>1,2,3</sup>, (Senior Member, IEEE), AFSANA AHSAN JENY<sup>1,2</sup>, AREZOO SADEGHZADEH<sup>1,2</sup>, TOPU BISWAS<sup>4</sup>, (Member, IEEE), AND A. F. M. SHAHEN SHAH<sup>1,5</sup>, (Senior Member, IEEE)

<sup>1</sup>Department of Computer Engineering, Daffodil International University, Dhaka 1207, Bangladesh

<sup>2</sup>Department of Computer Engineering, Bahçeşehir University, 34349 Istanbul, Turkey

<sup>3</sup>College of Data Science and Engineering, American University of Malta, 1013 Bormla, Malta

<sup>4</sup>Faculty of Engineering, Multimedia University, Cyberjaya 63100, Malaysia

<sup>5</sup>Department of Electronics and Communication Engineering, Yıldız Technical University, 34220 Istanbul, Turkey

Corresponding author: Masum Shah Junayed (masumshahjunayed@gmail.com)

This work was supported in part by the Scientific and Technological Research Council of Turkey (TUBITAK) under 2232 Outstanding Researchers Program, under Project 118C301.

**ABSTRACT** Acne scarring occurs in 95% of people with acne vulgaris due to collagen loss or gains when the body is healing the damages of the skin caused by acne inflammation. Accurate classification of acne scars is a vital factor in providing a timely, effective treatment protocol. Dermatologists mainly recognize the type of acne scars manually based on visual inspections, which are time- and energy-consuming and subject to intra- and inter-reader variability. In this paper, a novel automated acne scar classification system is proposed based on a deep Convolutional Neural Network (CNN) model. First, a dataset of 250 images from five different classes is collected and labeled by four well-experienced dermatologists. The pre-processed input images are fed into our proposed model, namely *ScarNet*, for deep feature map extraction. The optimizer, loss function, activation functions, filter and kernel sizes, regularization methods, and the batch size of the proposed architecture are tuned so that the classification performance is maximized while minimizing the computational cost. Experimental results demonstrate the feasibility of the proposed method with accuracy, specificity, and kappa score of 92.53%, 95.38%, and 76.7%, respectively.

**INDEX TERMS** Acne scars, dataset, image classification, CNN, skin disorder, skin image analysis.

## I. INTRODUCTION

Acne scars originate in the tissue damage resulting from the inflammatory acne lesions and Vulgaris, which may need long-time treatment to be removed [1]. Consequently, acne scars can be more troublesome for patients than acne vulgaris, and they may have substantial adverse psychological and emotional effects on the social life of the patients. It weakens the quality of the life and can lead to anger, depression, embarrassment, poor self-image, low academic performance, social withdrawal, and limited employment chances [2]. It is reported in Global Burden of Disease Project [3] that the prevalence rate of acne is 9.4% of the global population and identified as the 8<sup>th</sup> most common disease worldwide [4].

The associate editor coordinating the review of this manuscript and approving it for publication was Vishal Srivastava.

Almost over 90% of adolescents (i.e., 95-100% of boys aged 16-17 and 83-85% of girls aged 16-17) experience acne based on hormonal fluctuations, and it persists into adulthood (i.e., adults in their 40-50s) in about 12-14% of cases [5]. Due to the lack of dermatologists and the long-awaited time for an appointment (an average of 32 days) [6], patients do not receive timely acne treatments. This delay in starting the treatment process results in permanent, disfiguring acne scars because of some injuries in the sebaceous follicle.

There are numerous options available for acne scar treatment, such as chemical peels, laser treatment, punch techniques, cosmetic filler, dermabrasion/microdermabrasion, microneedling, onion extract, local tumescent, subcision, surgery, and combined therapies [1]. However, choosing the effective and appropriate option and its related protocols for ideal acne scar treatment highly depends on the acne

scar types and subtypes. Although several works have been reported for acne scar treatment in the literature, there have been only a few descriptive terms to diagnose the types of acne scars [1], [7], [8].

There are three main types of acne scars: atrophic, hypertrophic, and keloidal, among which atrophic is the most well-known type [7]. Atrophic scars are further subdivided into icepick, rolling scars, and boxcar [9], which results in totally five acne scar classes. For clinical purposes, dermatologists usually classify the acne scars into these five types based on a simple visual inspection (using the descriptive terms) by a direction or overhead light, a magnification/dermatoscope, and identification marks on patients' faces. Two quantitative scoring methods have also been proposed for acne scar grading [10], [11]. However, in these visual inspection-based methods, the classification process is time-consuming, has high error rates, and causes discomfort for patients. Additionally, as the descriptive methods are based on the textural irregularities and the physical characteristics of the scars, such as colors, shapes, patterns, width, depth, 3D architecture, etc., the classification results are highly subjective to the expert's experience and knowledge. Hence, to infer consistent treatments for acne scars, a unique accepted standard acne scar classification system is required to recognize the scar type efficiently and fast, with low cost and minimal dependence on expert help.

In the last decade, deep neural networks and machine learning techniques for medical image analysis, especially skin disease detection and classification such as acne vulgaris, cancer, etc., have received much attention [12]–[21]. Even a few studies were conducted for acne scar detection [22], [23]. However, there have been no AI-based automated acne scar classification systems to the authors' best knowledge. Generally, providing such a system is challenging due to several main reasons: (a) existence of many different human skin tones, (b) large variations in the appearances of acne scars such as their shape, size, and even the position of the scar, (c) dependency of the acne scars on the patients' age, gender, and skin types, and (d) the lack of an appropriate and publicly available dataset with a large number of images sufficient for learning-based methods (previously published datasets are only for acne vulgaris classification and grading [24]–[29], not for acne scar).

An acne scar dataset (with five classes) and an automated acne scar classification system based on a deep convolutional neural network (CNN) are proposed to address the issues and challenges mentioned above. Overall, the contributions and strengths of this work can be summarized as follows:

- An acne scar dataset named “*5-class Acne Scar*” has been created, including 250 images labeled in five classes of acne scar types by four experienced ophthalmologists. To the authors' best knowledge, “*5-class Acne Scar*” is the first dataset in this field that provides the images from five acne scar types of Hypertrophic, Keloidal, Icepick, Rolling, and Boxcar.

- As the first attempt, an automated computer-aided acne scar classification system is proposed based on a novel deep 19-layer CNN model, i.e., *ScarNet*. In this model, the activation function, optimization algorithm, loss function, kernel sizes, and batch size are adjusted to reduce the computational cost, such as model size, training parameters, and running time. At the same time, the accuracy is still high with a limited number of layers compared to the pre-trained models.
- To obtain the finest mass images, our dataset passes a pre-processing step, including image resizing, quality improvement, and augmentation. We benefit from the guided filter as a contrast enhancement technique to reduce the noise while preserving the edges of the acne scars. Additionally, to have a better representation of the acne images and approximate the human vision,  $L^*a^*b^*$  color space is applied, which results in competitive classification performance. Pre-processing step ends with augmentation, which increases the number of training samples five times to prevent model overfitting.
- According to the extensive availability of smartphones, the proposed system can be used by ordinary people, especially in underdeveloped countries (where there is a lack of dermatologists) as a remote screening system.
- Comparing the performance of *ScarNet* with four conventional machine learning (ML)-based classifiers, i.e., Decision Tree (DT), Multi-layer Perceptron (MLP), Support Vector Machine (SVM), and Random Forest, and five pre-trained deep learning-based models, i.e., Inception-V3, MobileNet, RedNet-50, AlexNet, and VGG-16 on the developed dataset, our model attains a competitive performance in acne scar classification with high accuracy and minimized computational cost.

The rest of the paper is organized as follows. In Section II, the recently reported studies related to skin diseases, especially acne vulgaris detection and classification, are reviewed. Data collection is presented in Section III. Section IV represents our proposed system in detail, including the pre-processing step and the architecture of our CNN model. The evaluation metrics, experimental setup and analysis, comparisons, and the related discussions are all presented in section V. Finally, section VI concludes the paper and provides our future research directions.

## II. RELATED WORKS

Although numerous approaches have been reported in the literature for skin image analysis, such as detection and grading of acne vulgaris, skin cancer, skin eczema, etc., in the last decade, the literature lacks computerized systems for automated acne scar classification. Generally, skin disease-related studies can be categorized into two main groups: (i) classical computer vision- and machine learning-based methods, and (ii) deep learning-based approaches. Some of the acne-related approaches are discussed briefly in this section.

## A. CONVENTIONAL APPROACHES

In conventional methods, the handcrafted features are extracted from the raw images and then employed for different processes such as detection and classification. In [30], acne and facial skin defect recognition system was proposed based on SVM classifier. After extracting the region of interest (ROI), particular color space and an adapted marginal area were used to distinguish possible defects from the ROI. Finally, specific important texture characteristics from 126 acne, 134 marks, and 134 regular skin patches were employed in the final classification of the experiments. Although it received an accuracy of 99.40%, it is time-consuming due to including multiple stages.

Dey *et al.* [23] proposed a system for detecting acne scar pixels based on color image processing. In this method, the knowledge base was created by recording pixels from skin as background and from acne scars as ROI. The segmentation was carried out using Mahalanobis distance (MD) based on the minimum-distance rule in the RGB space. Applying MD, average values of 90.36 and 93.82 were obtained for sensitivity and specificity, respectively. An acne grading method was presented in [31] based on SVM, which was applied to classify acne vulgaris into four classes, i.e., mild, moderate, severe, and very severe. Khongsuwan *et al.* [32] proposed a counting system for estimating the number of acne vulgaris as points on the skin whose prediction accuracy was 83.75%. Later, a mobile application was developed in [24] for acne vulgaris detection, classification, and segmentation evaluated on only 35 images in five classes. A binary classification (normal skin and acne) was performed based on Fuzzy C-Means (FCM) with an accuracy of 100%. Another binary classification task was conducted for distinguishing acne scar from inflammatory acne based on SVM and FCM with an average accuracy of 80% and 66.6%, respectively. However, for a proper evaluation, more images are required. Abas *et al.* [33] proposed a method for counting the number of lesions on a region of skin and segmenting them into six classes (5 classes of acne vulgaris types and one scar class). In their method, ROI is extracted based on entropy-based filtering and thresholding. Applying a binary classification tree and a combination of two descriptors, i.e., discrete wavelet and gray-level co-occurrence matrix, an accuracy of 85.5% was achieved.

An acne detection approach was presented in [34] based on applied speeded up robust features with an average accuracy of 68%. Recently, a hybrid acne vulgaris classification method has been proposed by Hameed *et al.* [27] based on Naive Bayes Classifier (NBC) and image processing on a dataset of 3 classes with 40 images in each. Their system obtained an accuracy of 93.42%. Generally, using machine learning techniques, e.g. K-means clustering and SVM, is complicated and challenging as the handcrafted features must be extracted before training the model. Additionally, the feature extraction and arrangements are task-subordinate and cannot be summed up easily. These methods also suffer from the lack of self-adaptivity due

to manual feature extraction. Although many conventional approaches have been published for acne vulgaris detection and classification, as far as we know, there are still no studies for acne scar classification, even based on these classical techniques.

## B. DEEP LEARNING-BASED APPROACHES

According to recent studies, the extracted features based on CNNs are deeper and more effective than hand-crafted features extracted by conventional techniques. Inspiring from this fact, the outstanding performance of CNNs, significant advancement in GPUs, and the availability of large datasets, deep neural networks have gained growing popularity and attracted much attention among researchers in medical image analysis. In [25], the skin images were first distinguished from non-skin images by applying a binary-classifier. Then seven different types of acne vulgaris were classified based on the features extracted from a CNN-based model. AcneNet was proposed by Junayed *et al.* [26] based on a Deep Residual Neural Network to recognize five types of acne vulgaris using a total number of 1800 images. Compared to two pre-trained models, i.e., Inception-V3 and MobileNet, their model received higher accuracy of 86.28% and 95.89% for training and testing, respectively, which shows a noticeable amount of underfitting in the training process.

A facial acne Vulgaris grading system was proposed by Zhao *et al.* [35] using 4,700 selfie images labeled in 5 classes of severity. First, the irrelevant background was removed to find facial landmarks through which the key skin patches were selected. Using the pre-trained ResNet-152 and transfer learning approach, the features were extracted from the images, fed into a fully connected layer for final classification. Chitransh *et al.* [36] utilized five classifiers such as Logistic Regression, Random Forest, Kernel SVM, Naive Bayes, and CNN to detect three different types of skin diseases, precisely, Acne, Lichen Planus, and Stevens-johnson syndrome (SJS) and toxic epidermal necrolysis (TEN). Among these classifiers, CNN performed better than other machine learning algorithms. The accuracy of Logistic Regression, Random Forest, Kernel SVM, Naive Bayes, and CNN were 73.76%, 73.36%, 50.7%, 49%, and 99.05%, respectively.

Junayed *et al.* [37] proposed a deep CNN model to recognize and classify five types of Eczema diseases using 2500 images with an accuracy of 96.2%. Despite the high accuracy, it suffered from overfitting as around 24M parameters were utilized in their proposed model with no dropout layers. The acne vulgaris classification performance of the Faster Region-based CNN (Faster R-CNN) and Region-based Fully Convolutional Network (R-FCN) were compared by Rashataprucksa *et al.* in [29] using 871 images in four classes. A mean average precision of 28.3% was obtained for R-FCN, which is still low for real-life clinical applications. Although the deep learning-based methods have been extensively developed and applied in medical

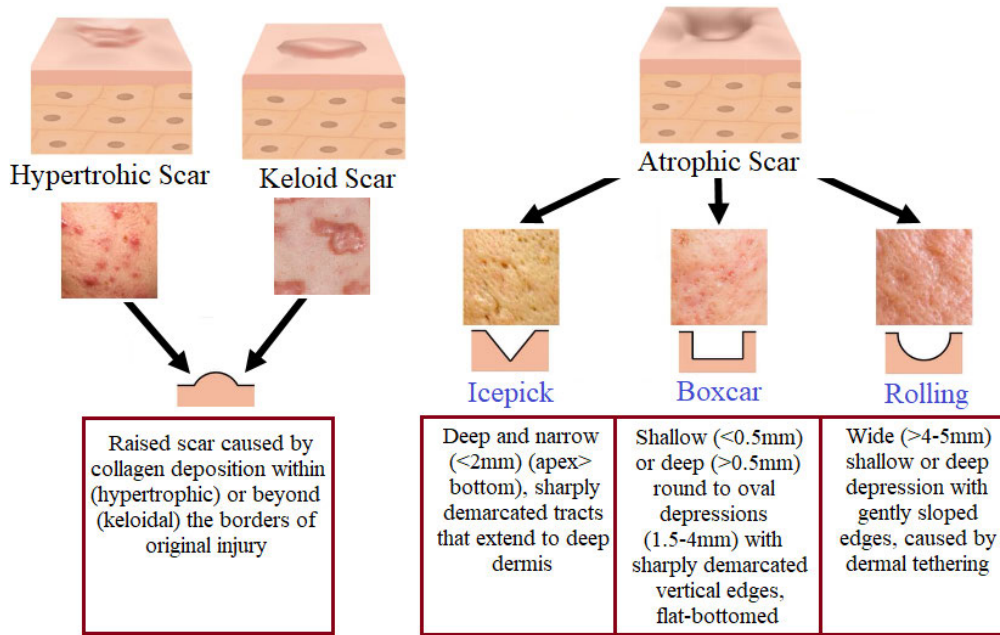


**FIGURE 1.** Samples from five different types of acne scars and their characteristics, i.e. Hypertrophic, Keloid, Icepick, Boxcar, and Rolling scars.

image analysis (i.e., skin disease detection and acne vulgaris detection, grading, and classification), there is still a lack of an automated acne scar classification system.

### III. DATASET DEVELOPMENT

Acne scars are the secondary lesions of acne vulgaris formed by the natural reaction of body tissue while healing the existed injuries. Depending on the net loss or gain of collagen in the tissue in the healing process, there are two basic types of acne scars [7]: atrophic and hypertrophic/keloidal scars, respectively. The most common ones are atrophic acne scars, further divided into three sub-classes of rolling, icepick, and boxcar. All these five types are illustrated in Fig. 1 and their main characteristics are presented as follows:

**Rolling:** they are typically more extensive than 4 to 5 mm. Having a varying depth, these spots create an “M” shape with sloping edges giving the skin a wavy and uneven appearance.

**Icepick:** they are “V”-shaped, more narrow, and profound, pointing down into the skin, which mostly appears on the cheeks. The treatment of this type of scar is callous and requires a continuous process.

**Boxcar:** they are broad, box-shaped scars like a “U” with a wide base and sharp vertical edges mostly caused by chickenpox, virus-based rash, widespread acne vulgaris, or varicella. They commonly appear on the thick part of the skin, such as the lower cheeks and jaw.

**Hypertrophic:** typically, these scars are pink, raised tissue on the skin that stays inside the actual acne’s boundaries, which means they have the same size as the acne from which they are originated. They commonly appear on the darker skin color on the chest, shoulders, back, and jawline areas.

**Keloidal:** these are raised scars very similar to hypertrophic. The only difference is that keloidal spots are more

significant than the initial acne and propagate beyond their limits.

The degrees of all types of acne scars are increased if they receive delayed treatment [38]. There have been numerous treatment methods for acne scarring, among which the most effective and suitable treatment options can be selected based on the type of the scar [8]. For instance, Rolling acne scars can be treated by the picosure laser or trichloride acid peel, while punch excisions and AFL are helpful and effective treatments for Icepick scars [39]. It is also true about home treatment. For example, atrophic acne scars can be successfully treated at home with topical over-the-counter (OTC) retinoids, such as Differin. In contrast, hypertrophic and keloid scars are softened, and their height is reduced using gel silicone sheets. Hence, it is vital to have an automated acne classification system with highly accurate performance for timely treatment.

One of the significant and challenging factors in applying computer-aided techniques, especially the deep learning-based ones, to clinical applications is getting access to a proper dataset with sufficient images already labeled by a health professional. There is still no publicly available dataset for acne scar classification in the literature to the authors’ best knowledge. To overcome this challenge and fill this gap between the research and medical applications, a dataset of 250 RGB images in 5 different classes of acne scars (each class contains 50 images), namely “*5-class Acne Scar*”<sup>1</sup>, is proposed. Among them, 51 images have been captured by the authors from the visited patients to the Dhaka

<sup>1</sup>The dataset is available at <https://bit.ly/3J8hWDx>. For any issues regarding downloading the dataset, please contact [mamumshahjunayed@gmail.com](mailto:mamumshahjunayed@gmail.com) or [bislam.eng@gmail.com](mailto:bislam.eng@gmail.com).



**FIGURE 2.** Sample images from our developed acne scar dataset “5-class Acne Scar”, the rows from top to bottom represent the acne scar classes of rolling, icepick, boxcar, hypertrophic, and keloidal, respectively.

Medical College (DMC) hospital by a 48-MP camera of a smartphone. These data were collected by following the individual patient’s consent. The remaining 199 images were gathered from online sources especially from DermNet [40]. All the images, either collected online or captured by the authors, have been all labeled in five different classes by four well-experienced dermatologists to obtain more reliable labels and so high performance accuracy. Some samples of these five classes in our dataset are illustrated in Fig. 2.

#### IV. PROPOSED SCARNET METHOD

The main flowchart of the proposed acne scar classification system is illustrated in Fig. 3. First, the images of our developed dataset are passed a pre-processing step. The pre-processed images are fed into a CNN-based model for feature extraction as well as classification. The details of each step are presented in the following subsections.

##### A. PRE-PROCESSING

The quality of the input images can significantly affect the performance of the whole system. Hence, image pre-processing is essential to improve the image quality and have more accurate subsequent image analysis processes such as classification. The pre-processing module comprises three sub-modules in our proposed method: image resizing, image quality improvement, and augmentation. Before applying the two latter sub-modules, the images of the developed dataset are all resized to  $224 \times 224$  pixels.

##### 1) IMAGE QUALITY IMPROVEMENT

One of the main factors in medical image analysis is improving the contrast of the images for providing a better

representation. Hence, in our proposed system, guided image filtering [41] is employed as contrast enhancement to reduce the noise of the input images while preserving the edges of the acne scars. This enhancement in the edges of the scars makes it easier for the model to train different acne scars and distinguish between them. The guided filter is similar to conventional bilateral filter [42] as an edge-preserving smoothing operator but with a difference that it has a better performance close to the edges with a fast and non-approximate linear-time algorithm. In this algorithm, the filtering size has no impact on the computational complexity, and the performance is outstanding both in quality and efficiency. It is assumed that there is a linear relationship between the guidance  $I$  and the filter output  $q$  since the object edges depend on its gradient. If  $q$  is a linear transformation of  $I$  in a window  $w_k$  ( $k$  is the center pixel), the basic model of the guided filter is as follows [41]:

$$\begin{aligned} q_i &= a_k I_i + b_k, \quad \forall i \in w_k \\ q_i &= p_i - n_i \end{aligned} \quad (1)$$

where  $(a_k, b_k)$  are some constant linear coefficients in  $w_k$  (a square window of a radius  $r$ ),  $q_i, p_i, n_i$ , and  $I_i$  are output pixel, input pixel, pixel of noise components, and guidance image pixel, respectively. As  $\nabla q = a \nabla I$ , it is guaranteed that  $q$  has an edge only if  $I$  contains an edge. Some samples of contrast enhancement on the images of the developed dataset are illustrated in Fig. 4 (second column).

Once the contrast enhancement is applied by guided filter on the images, their color space is converted from RGB to  $L^*a^*b^*$  to provide a better representation of acne scar regions and so achieve a better classification accuracy. In the color-opponent  $L^*a^*b^*$  color space,  $L^*$  is for lightness and  $a^*$  and  $b^*$  are for the color-opponent dimensions according to the CIE XYZ color space coordinates which are compressed nonlinearly [43]. In comparison to the RGB and CMYK colour models,  $L^*a^*b^*$  colour space is created to approximate human vision.  $L$  component highly matches the human perception of lightness so that it can be utilized to adjust the lightness contrast or to form the accurate color balance corrections by changing and improving the output curves in the  $a$  and  $b$  components. In contrary, RGB or CMYK spaces do not model the human visual perception and they show the output of physical devices. Hence, in these spaces, the mentioned transformations can be only realized by editing applications and applying appropriate blend modes. Consequently, in our proposed method, the color space of the images are converted from RGB to  $L^*a^*b^*$ . Through this conversion, a better representation is provided from the input images and the acne scar regions which significantly enhances the final classification accuracy. Some samples of  $L^*a^*b^*$  color space conversion on the images of the developed dataset are illustrated in Fig. 4.

##### 2) AUGMENTATION

In deep learning-based models, one of the critical factors is providing a considerable number of training images.

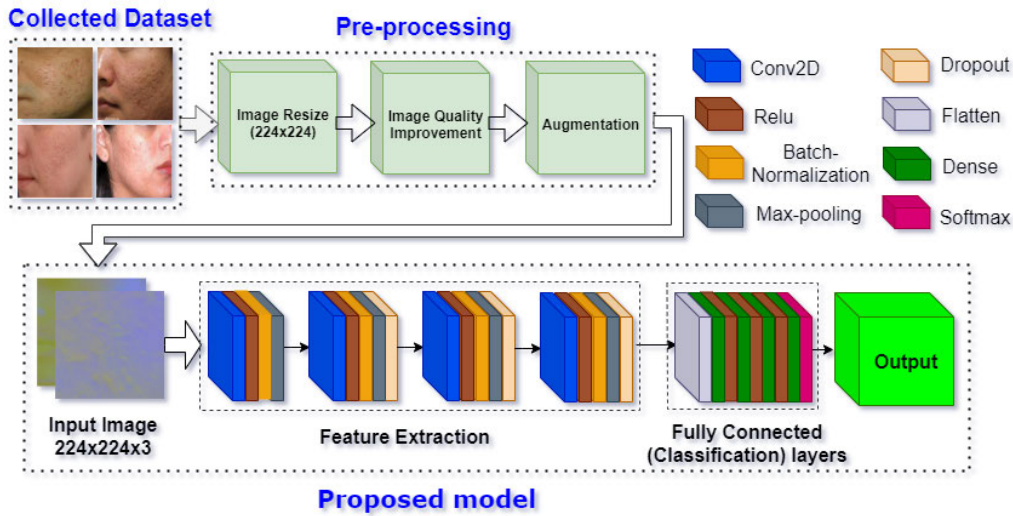


**FIGURE 3.** The overview of the proposed *ScarNet* model for acne scar classification is composed of a pre-processing module and CNN-based feature extraction and classification.

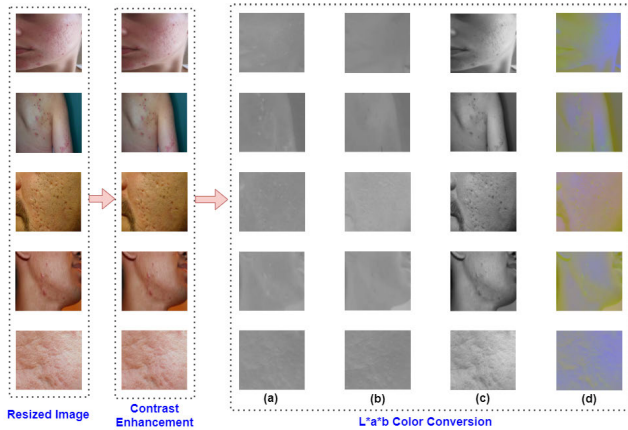


**FIGURE 4.** Some samples of image quality improvement in the proposed *ScarNet* include contrast enhancement by guided filter and  $L^*a^*b^*$  color space conversion. (a), (b), and (c), are  $L^*$ ,  $a^*$ ,  $b^*$ , and combinations of  $L^*a^*b^*$  layers, respectively.

The original proposed five-class dataset is relatively small; thus, the neural network might face an overfitting problem during training or not be robust to different input patterns. Hence, five other data augmentation techniques, i.e., randomly rotating  $30^\circ$  to left or right, horizontal flipping, shearing, scaling, and translation, are applied to the training samples to produce additional images equal to five times the original ones. Increasing the number of training data prevents the model from overfitting and improves the performance of the system. To delve deeply into the details of the augmentation techniques, a transformation matrix is utilized to represent the augmentation methods as follows:

$$X = \begin{bmatrix} L & M & N \\ O & P & Q \\ R & S & T \end{bmatrix} \quad (2)$$

where,  $L$  and  $P$  regulate the image scaling,  $N$  and  $Q$  regulate the translation of the image,  $M$  and  $O$  regulate the shearing

of the image. In detail, the rotation part of the transformation matrix is considered as:

$$X = \begin{bmatrix} \cos\alpha & -\sin\alpha & -\cos\alpha \frac{u+1}{2} + \sin\alpha \frac{v+1}{2} + \frac{u+1}{2} \\ \sin\alpha & \cos\alpha & -\sin\alpha \frac{u+1}{2} - \cos\alpha \frac{v+1}{2} + \frac{v+1}{2} \\ 0 & 0 & 1 \end{bmatrix} \quad (3)$$

where,  $u$ ,  $v$ , and  $\alpha$  are the picture's height, width, and rotation angle, respectively. The translation part of the transformation matrix is:

$$X = \begin{bmatrix} 1 & 0 & z_a \\ 0 & 1 & z_b \\ 0 & 0 & 1 \end{bmatrix} \quad (4)$$

where,  $z_a$  and  $z_b$  are the height and width for translation. The shearing is defined as:

$$X = \begin{bmatrix} 1 & -\sin\mu & -j_a \frac{u+1}{2} + \frac{u+1}{2} \\ 0 & \cos\mu & -\frac{u+1}{2} - \cos\mu \frac{v+1}{2} + \frac{v+1}{2} \\ 0 & 0 & 1 \end{bmatrix} \quad (5)$$

where,  $\mu$ ,  $u$ , and  $v$  are the transformation intensity, the height, and the width of shearing, respectively. Scaling of the images is as:

$$X = \begin{bmatrix} j_a & 0 & -j_a \frac{u+1}{2} + \frac{u+1}{2} \\ 0 & j_b & -j_b \frac{v+1}{2} - \frac{v+1}{2} \\ 0 & 0 & 1 \end{bmatrix} \quad (6)$$

where,  $j_a$  and  $j_b$  regulate the zooming scales of the image.

**TABLE 1.** The summary of the ScarNet architecture including layers, filter sizes, their configurations (kernel sizes, activation functions, etc.), and the output shape of each layer.

Layer	Filter	Config.	Stride	Output
Conv2D	64	KS: 5 × 5; Relu	2	224 × 224 × 64
BatchNormalization	-	-	-	224 × 224 × 64
Max-pooling2D	-	KS: 2 × 2	2	112 × 112 × 64
Conv2D	48	KS: 3 × 3; Relu	2	112 × 112 × 48
BatchNormalization	-	-	-	112 × 112 × 48
Max-pooling2D	-	KS: 3 × 3	2	56 × 56 × 48
Dropout	-	0.4	-	56 × 56 × 48
Conv2D	32	KS: 3 × 3; Relu	2	56 × 56 × 32
BatchNormalization	-	-	-	56 × 56 × 32
Max-pooling2D	-	KS: 2 × 2;	2	28 × 28 × 32
Dropout	-	0.4	-	28 × 28 × 32
Conv2D	16	KS: 3 × 3; Relu	2	28 × 28 × 16
BatchNormalization	-	-	-	28 × 28 × 16
Max-pooling2D	-	KS: 2 × 2	2	14 × 14 × 16
Dropout	-	0.25	-	14 × 14 × 16
Flatten	-	-	-	-
Dense	-	512; Relu	-	512
Dense	-	256; Relu	-	256
Dense	-	128; Relu	-	128
Softmax	-	5	-	5

## B. MODEL ARCHITECTURE

In recent years, various CNN models have been widely used to detect and classify 2D, and 3D images [44]–[46] thanks to the existence of the significant number of data and high GPUs. CNN-based models divert scientists' attention away from traditional machine learning approaches in favor of higher performance, quality, and speed [47].

A novel multi-layer deep CNN model, namely *ScarNet*, is proposed for acne scar classification with minimum computational cost. It is composed of a total of 19-layers whose details are presented in Table 1. Total 15-layers are placed in four convolution blocks, and the remaining 4-layers are fully connected layers applied for classification. The input images of the first convolution block are  $224 \times 224 \times 3$  images in  $L^*a^*b^*$  color space. All convolution blocks contain a convolutional layer, a Batch Normalization (BN) layer, and a Max-polling (MP) layer. The applied filters in four convolutional layers are 64, 48, 32, and 16, respectively, with a kernel size (KS) of  $5 \times 5$  in the first block and  $3 \times 3$  in the other three blocks. As the large-sized images with a high number of pixels need more training parameters and more space size, a Max-Pooling (MP) layer is designed in all blocks. The employed KS for the MP layer in all blocks is  $2 \times 2$  except in the second block, which is  $3 \times 3$ . In all convolutional and MP layers, zero-padding (i.e., allocating 0 values around the inputs to keep the output size equal to every kernel filter input for each convolution process) is applied with a stride of 2. BN and dropout layers are employed as regularization layers to improve the convergence, enhance the generalization, reduce the overfitting, and obtain a better performance on invisible information. BN layer is used in all four blocks while a dropout layer is applied only in each of the last three blocks setting as 0.4, 0.4, and 0.25 (i.e., 40%, 40%, and 25% of neurons in the hidden layers are considered as 0 at each training update).

The features of the input images are extracted as feature maps by passing these four blocks. The generated feature maps are fed into the last four fully connected layers, i.e., a flatten layer, three dense layers (with 512, 256, and 128 neurons, respectively), and one softmax layer, for final acne scar classification into five different classes. Rectified Linear Unit (ReLU) is used in all convolutional and dense layers as a nonlinear activation function:

$$\text{Relu} = \max(0, x) \quad (7)$$

This function means that the value of 0 will be assigned if the input value is a non-positive value. Otherwise, its value remains unchanged. The last activation function of our proposed model is the softmax function which is a generalization of the logistic function to multiple classes. Through this function, the network output is normalized to a probability distribution over the predicted output classes as follows:

$$S(Z)_i = \frac{e^{z_i}}{\sum_{j=1}^K e^{z_j}} \quad \text{for } i = 1, 2, \dots, K \quad (8)$$

where  $z$  is the input vector of  $K$  real numbers (number of classes) which is normalized into a probability distribution including  $K$  probabilities proportional to the exponentials of the input numbers. Hence, before the softmax function, the sum of vector components might not be 1 because there might be a negative or greater than one value. Once the softmax is applied, all the values are normalized in an interval of  $[0, 1]$ . Thus, the sum of the components of the output vector  $S(Z)_i$  is guaranteed 1. In our model, the softmax function allocates distributions of probability to produce predictions for each acne scar class prediction. The training process is optimized using Adam Optimizer, which minimizes the error of the CNN model and makes it more reliable and efficient. The adopted learning rate and batch size are 0.0001 and 32.

## V. EXPERIMENTAL RESULTS AND DISCUSSION

In this section, the experimental setup, evaluation metrics, and the results are presented. The effects of the augmentation, the batch size, the guided filter, and the  $L^*a^*b^*$  color space conversion on the final classification accuracy are also investigated. Additionally, the performance of the *ScarNet* is compared with four conventional ML-based classifiers and five pre-trained models on our developed dataset.

### A. EXPERIMENTAL SETUP

Experiments are carried out using a 3.60 GHz Intel Core i9-10850K CPU, 64 GB RAM, and an NVIDIA GeForce RTX 2080 GPU with 8GB video memory. Pre-processing, designing the CNN architecture, and training and testing are conducted in Python, Keras, and Tensorflow platforms.

### B. EVALUATION CRITERIA

To evaluate the performance of our proposed method, six different evaluation metrics are employed, i.e. accuracy ( $\frac{TP+TN}{TP+TN+FP+FN}$ ), Recall/Sensitivity ( $\frac{TP}{FN+TP}$ ), Precision

**TABLE 2. Performance comparison of the proposed ScarNet for five different dataset splitting scenarios.**

(Train - Test)	Accuracy (%)	Precision (%)	Recall (%)	F1-Score (%)
(90 - 10) %	89.34	71.67	74.14	72.88
<b>(80 - 20) %</b>	<b>92.53</b>	<b>81.33</b>	<b>82.24</b>	<b>81.38</b>
(70 - 30) %	91.30	76.27	78.95	77.59
(60 - 40) %	89.67	75.01	73.77	74.38
(50 - 50) %	88.04	68.33	70.69	69.49

( $\frac{TP}{TP+FP}$ ), F1-score ( $2 \times \frac{Precision \times Recall}{Precision+Recall}$ ), Kappa ( $k = \frac{2 \times (TP \times TN - FN \times FP)}{(TP+FP) \times (FP+TN) + (TP+FN) \times (FN+TN)}$ ), and Specificity ( $\frac{TN}{FP+TN}$ ). These evaluation metrics are defined based on confusion matrix in which TP, TN, FP, and FN refer to True Positive (both real and predicted classes are 1 (True)), True Negative (both real and predicted classes are 0 (False)), False Positive (the actual class of the data is 0 while the predicted one is 1), and False Negative (the actual class of the data is 1 while the predicted one is 0), respectively. The reason behind choosing False as the name is that the prediction done by the model is incorrect. To define these metrics in detail, accuracy is the number of correct predictions over the total number of predictions, also called classification rate. Recall/Sensitivity determines the correctly identified actual positive values, which is known as true positive rate. The number of predicted positive classes which belong to the actual positive class is calculated by precision. F1-score measures the testing accuracy. Finally, Kappa is a rigorous method of finding the degree of agreement between two raters/judgments, categorizing  $N$  items into  $C$  categories.

### C. PERFORMANCE ASSESSMENT

The performance of the proposed ScarNet is evaluated in terms of accuracy, precision, recall, specificity, and F1-Score. Images in the dataset are resized into  $224 \times 224$  pixels whose quality is then improved by passing a guided filter and converting the color space from RGB to  $L^*a^*b^*$ . Splitting the pre-processed dataset into training, validation, and testing sets, five different augmentation techniques are applied to the training set to increase the dataset number and prevent the model from overfitting and make it robust for future testing data with different variations. Five different dataset splitting scenarios are investigated with 90-10%, 80-20%, 70-30%, 60-40%, and 50-50%. The first value is for training and validation sets, and the second is for the test set. The performance of our system in terms of accuracy, precision, recall, and F1-score is presented in Table 2 for all five dataset splitting. Highlighting the best performance in bold, Our proposed system ranks first for 80-20% splitting condition in all mentioned four evaluation metrics with the values of 92.53%, 81.33%, 82.24%, and 81.38%, respectively. Hence, our experiments are based on an 80-20% splitting strategy. A total of 200 images (80%) of the dataset is used for training and validation. The rest 50 images (20%) are employed in the testing phase. It is worth mentioning that the five augmentation techniques are applied on the training set, which results in additional images equal to 5 times the original training set.

One of the critical hyperparameters required to be tuned in deep learning-based models is the batch size. It is mostly preferred by the researchers to utilize a larger batch size for training since it speeds up the computations. Adopting smaller batch sizes provides reasonable solutions with faster convergence, but there is no guarantee that the model converges to the global optima. Hence, to choose the best batch size with the number of epochs, we start our experiments at a small batch size of 16, which then increases to 32 and 64 to provide a significant trade-off between faster training dynamics and guaranteed convergence. The performance of the proposed CNN-based model is evaluated with training and validation sets for five different epoch numbers of 10, 20, 30, 40, and 50, and three different batch sizes of 16, 32, and 64. The results in terms of training accuracy (TA), validation accuracy (VA), training loss (TL), and validation loss (VL) are presented in Table 3. The highest performance is achieved for 50 epochs and the batch size of 32 with TA, VA, TL, and VL equal to 88.02%, 86.33%, 0.51, and 0.50, respectively.

Figure 5 (a) and (b) demonstrate the training and validation accuracy and loss, respectively, for the optimized number of epochs and batch size (i.e. 50 and 32) in our proposed ScarNet. The X-axis is the number of epochs in both graphs, while the Y-axis represents the accuracy or loss values. Initially, the training and validation accuracy is around 63% and 71%, respectively. Once 40 epochs pass, both graphs flatten out and reach the values of about 88% and 86%, respectively. However, there are some fluctuations in the validation accuracy before reaching its final value. The training and validation losses start from the values of about 0.66 and 0.83, respectively. Passing about 2 epochs, the validation loss dramatically decreases to 0.53. After two epochs, training and validation loss values decrease until they reach their least value of around 0.5. Considering both graphs, our proposed model performs without facing underfitting or overfitting problems.

The proposed ScarNet is evaluated on the test set, and the results are presented for all five acne scar classes separately in Table 4 in terms of accuracy, precision, recall, specificity, and F1-score. The highest accuracy, recall, and F1-score values are attained by Icepick with the values of 94.67%, 87.50%, and 86.67%, respectively. In two other metrics of precision and specificity, Rolling scar ranks first with the values of 88.33% and 96.86%, respectively.

### D. THE EFFECTS OF $L^*a^*b^*$ COLOR SPACE CONVERSION

To deeply analyze the effectiveness of the  $L^*a^*b^*$  color space conversion on the accuracy of the proposed system, the performance of the system is also evaluated without applying the color space conversion. To this end, the input RGB images are directly fed into our proposed CNN-based feature extractor after resizing, contrast enhancement, and augmentation. The experimental results of the ScarNet without applying  $L^*a^*b^*$  color space conversion are presented in Table 5. Comparing these results with those presented in



**TABLE 3.** The performance of the ScarNet is shown for five epoch numbers with three batch sizes in terms of TA (training accuracy), VA (validation accuracy), TL (training loss), and VL (validation loss).

Epoch	Batch Size 16				Batch Size 32				Batch Size 64			
	TA (%)	VA (%)	TL	VL	TA (%)	VA (%)	TL	VL	TA (%)	VA (%)	TL	VL
10	62.77	71.61	1.23	1.82	82.7	82.1	0.54	0.48	69.12	59.89	1.59	1.32
20	69.53	74.38	1.02	1.35	82.31	86.23	0.53	0.49	71.91	61.87	1.44	1.23
30	75.64	77.51	0.87	1.12	86.87	85.07	0.53	0.48	73.15	62.74	1.3	1.08
40	78.44	79.37	0.75	0.98	87.54	85.61	0.52	0.47	76.56	64.17	1.15	0.82
<b>50</b>	80.44	83.51	0.68	0.91	<b>88.02</b>	<b>86.33</b>	<b>0.51</b>	<b>0.50</b>	22.67	67.65	0.91	0.61

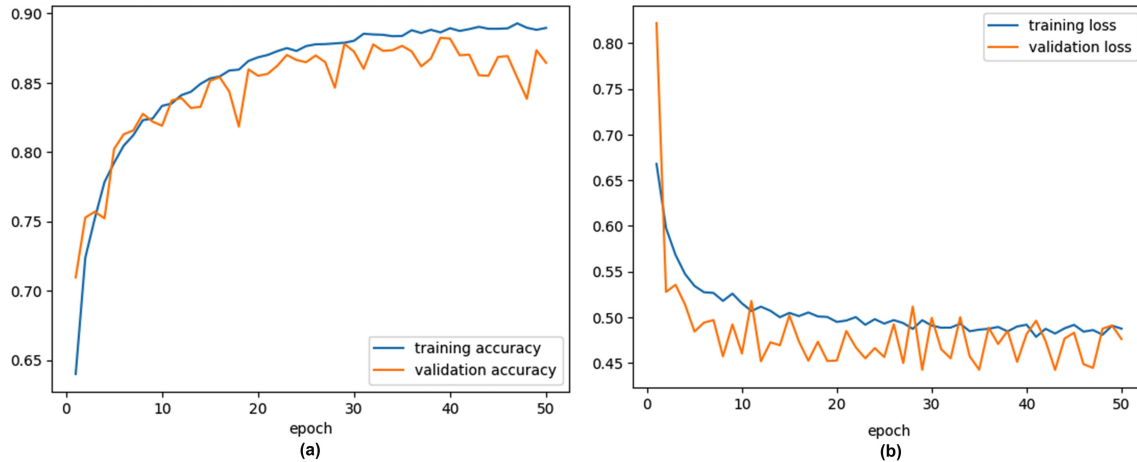


**FIGURE 5.** Training and validation (a) accuracy and (b) loss graphs of the proposed ScarNet.

**TABLE 4.** The performance of the ScarNet for each scar class and their average values in terms of accuracy (Acc), precision (Pre), recall (Rec), specificity (Spe), and F1-Score.

	Acc (%)	Pre (%)	Rec (%)	Spe (%)	F1-Score (%)
Boxcar	93.00	80.00	84.21	95.06	82.05
Hypertrophic	91.33	70.00	84.00	92.80	77.37
Ice Pick	<b>94.67</b>	86.67	<b>87.50</b>	96.67	<b>86.67</b>
Keloid	94.00	81.67	86.67	95.49	84.48
Rolling	89.67	<b>88.33</b>	68.83	<b>96.86</b>	76.36
Average	92.53	81.33	82.24	95.38	81.38

**TABLE 5.** The performance of the ScarNet in absence of  $L^*a^*b^*$  color space conversion in terms of five evaluation metrics (best results are presented in bold).

	Acc (%)	Pre (%)	Rec (%)	Spe (%)	F1-Score (%)
Boxcar	89.61	77.25	81.44	91.67	78.97
Hypertrophic	87.14	67.32	81.78	90.53	75.01
Ice Pick	91.36	85.08	84.19	93.98	<b>84.30</b>
Keloid	<b>91.76</b>	78.89	<b>84.52</b>	93.00	81.87
Rolling	86.90	<b>86.06</b>	66.95	<b>94.48</b>	74.41
Average	89.35	78.92	79.78	92.73	78.91

Table 4 for ScarNet using the  $L^*a^*b^*$  color space conversion demonstrates that  $L^*a^*b^*$  color space conversion improves the average performance 3.18% (from 89.35% to 92.53%), 2.41% (from 78.92% to 81.33%), 2.46% (79.78% to 82.24%), 2.65% (92.73% to 95.38%), 2.47% (78.91 to 81.38%) in terms of accuracy, precision, recall, specificity, and F1-score, respectively. Almost 2.5% enhancement in all performance evaluation metrics proves the effectiveness and significant influence of the  $L^*a^*b^*$  color space conversion on accurately recognizing the acne scar type by quantifying the visual differences and providing a better representation of the skin disease areas in the input images.

**E. THE EFFECTS OF GUIDED FILTER**

In the computerized systems specially in the field of medical image analysis, the quality of the input images highly influence the performance accuracy of the system. Generally, the quality of the images is improved by passing a pre-processing step to provide a better representation of the images. In our proposed system, the contrast of the input images is enhanced by passing a guided filter. Through this filter, the noise is reduced while the edges of the scars are preserved and enhanced. To investigate the impact of this quality enhancement on the overall performance of the system, it is evaluated without applying the guided filter and the results are presented in Table 6. Comparing these results with those presented in Table 4 (with guided filter) demonstrates that guided filter improves the average performance 1.52% (from 91.01% to 92.53%), 1.36% (from 79.97% to 81.33%), 1.51% (80.73% to 82.24%), 1.51% (93.87% to 95.38%), 1.16% (80.22 to 81.38%) in terms of accuracy, precision, recall, specificity, and F1-score, respectively. There is an average enhancement of 1.41% enhancement in all performance evaluation metrics which proves the effectiveness and significant influence of guided filter on better distinguishing between different types of acne scars.

**F. COMPARISON WITH DIFFERENT CLASSIFIERS**

To prove the capability of the classification layers of our proposed CNN-based ScarNet, the acne scar classification is conducted with four different machine learning classifiers

**TABLE 6. The performance of the ScarNet in absence of guided filter in terms of five evaluation metrics (best results are presented in bold).**

	Acc (%)	Pre (%)	Rec (%)	Spe (%)	F1-Score (%)
Boxcar	91.85	79.01	82.19	92.76	80.90
Hypertrophic	89.25	68.80	82.86	91.14	75.98
Ice Pick	92.69	84.51	<b>85.83</b>	94.99	<b>85.20</b>
Keloid	<b>92.87</b>	80.52	85.42	94.96	83.58
Rolling	88.40	<b>87.00</b>	67.33	<b>95.50</b>	75.45
Average	91.01	79.97	80.73	93.87	80.22

**TABLE 7. Performance comparison of the proposed ScarNet is shown with different machine learning-based classifiers.**

Classifiers	Accuracy	Precision	Sensitivity	Specificity
DT	84.97%	74.23%	73.07%	84.69%
MLP	85.44%	74.32%	73.91%	85.58%
SVM	87.93%	76.11%	74.96%	87.88%
Random Forest	89.17%	78.41%	77.59%	91.85%
<i>ScarNet</i>	<b>92.53%</b>	<b>81.33%</b>	<b>82.34%</b>	<b>95.38%</b>

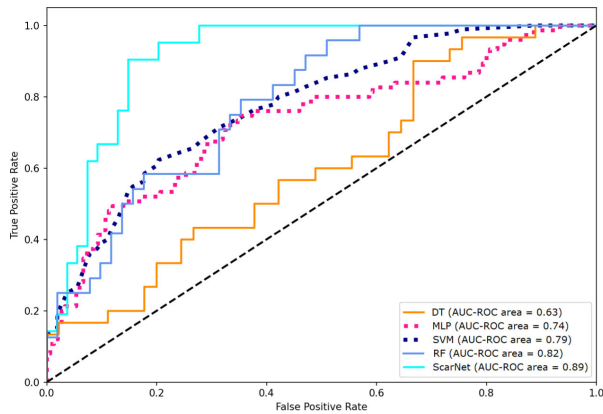


**FIGURE 6. The AUC of the ROC curves belonging to the ScarNet and four ML-based classifiers is shown. Each line indicates the performance of each classifier.**

and compared with the performance of our system. To follow this, the fully connected layers and the softmax layer, which are considered the classifier of our system, are replaced with machine learning-based classifiers: DT, MLP, SVM, and the Random forest. The extracted feature maps from four convolution blocks of *ScarNet* are fed into these classifiers. The performance of these classifiers is evaluated and compared with our classification system based on the softmax classifier in terms of accuracy, precision, sensitivity, and specificity in Table 7. Our model outperforms all four classifiers in terms of all evaluation metrics with the values of 92.53% (accuracy), 81.33% (precision), 82.34% (sensitivity), and 95.38% (specificity). Comparing the accuracy of DT (84.97%), MLP (85.44%), SVM (87.93%), and random forest (89.17%), our proposed *ScarNet* achieves at least 3.36% more accuracy than others.

As another evaluation tool, the performance of our system is compared with four classifiers based on the Receiver Operating Characteristic (ROC) Curve as illustrated in Fig. 6. It illustrates the trade-off between the true positive rate (TPR) as the y-axis and the false positive Rate (FPR) as the x-axis at different thresholds. The AUC (area under the curve)

indicates the classification capability in this probability curve by determining whether the curve is above or below the diagonal line (chance level). The AUC scores of the DT, MLP, SVM, RF, and the proposed *ScarNet* are 0.63, 0.74, 0.79, 0.82, and 0.89, respectively. Since a larger AUC indicates the greater performance, our proposed *ScarNet* surpasses the others with a maximum AUC of 0.89. The ROC curve for each of the acne scar classes based on the *ScarNet* is illustrated in Fig. 7. The AUC of all the classes is almost 0.9 except for Rolling wholes AUC is slightly less than the others (i.e. 0.86). These high values of AUC even in individual classes prove the high capabilities of *ScarNet*.

**G. COMPARISON WITH PRE-TRAINED MODELS**

To further prove the capability and efficiency of our proposed *ScarNet*, it is compared with five pre-trained models, i.e. Inception-v3 [48], MobileNet [49], VGG-16 [50], ResNet-50 [51], and AlexNet [52], on our proposed dataset in Table 8. Considering two scenarios for the dataset, i.e., training set with and without applying augmentation, the impact of the augmentation on the system’s performance is also investigated. The results are compared in terms of accuracy, precision, recall, specificity, and kappa score. First, comparing the results of all models in two dataset scenarios, it is observed that the accuracy is increased at least 10% after applying the augmentation. The performance of our proposed *ScarNet* before augmentation is 81.89%, 54.02%, 53.46%, 54.79%, and 53.60% in terms of accuracy, precision, recall, specificity, kappa score, respectively. After augmentation, these values are significantly increased to 92.53%, 81.33%, 82.24%, 95.38%, and 76.70%, respectively. Similar improvements are observed in the other pre-trained models as well due to augmentation. Hence, it is concluded that the augmentation can extremely improve the classification accuracy and prevent the model from overfitting. It also makes the system robust for the possible various future test data. Moreover, the proposed system outperforms the other five pre-trained models in all evaluation metrics in both with and without augmentation scenarios.

Our proposed model is also compared with the other pre-trained models in terms of network characteristics such as model size, training parameters, number of layers, number of epochs, and running time is Table 9. Our *ScarNet* not only achieves the highest classification accuracy but also has the most diminutive model size and the training parameters (18 MB and 0.89M, respectively). The largest model size belongs to VGG-16, with a value of 528MB. Our model achieves competitive performance by providing only 19 layers in 50 epochs (1/4 of the other models’ epochs). In contrast, the number of the layers increases even up to 177 in ResNet-50. The running time of our model is 217s which is at least five times less than those of other pre-trained models. These outstanding values for the network parameters of our CNN-based model and its superior performance prove

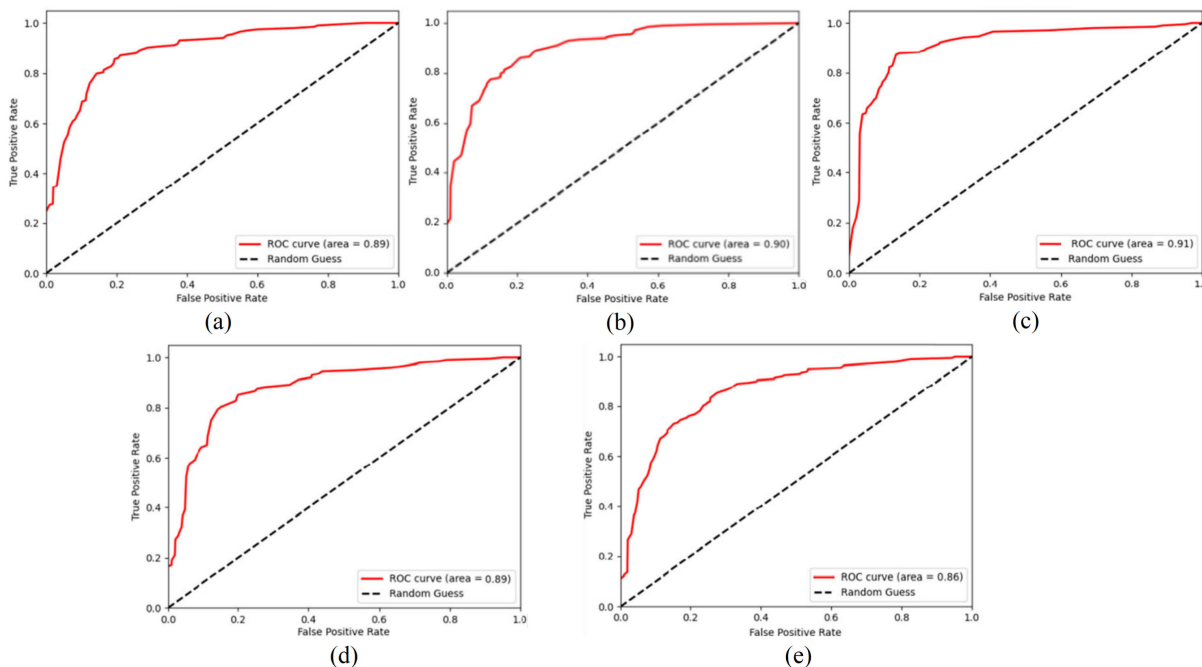


**FIGURE 7.** The AUC of the ROC curves belonging to each class of acne scars based on ScarNet. Here, (a), (b), (c), (d), and (e) represents the corresponding curves for Boxcar, Hypertrophic, Ice Pick, Keloid, and Rolling.

**TABLE 8.** Performance comparison with and without data augmentation between the proposed ScarNet and five pre-trained models on the developed dataset is shown.

Dataset	Models	Accuracy (%)	Precision (%)	Recall (%)	Specificity (%)	Kappa (%)
Without (augmentation)	Inception-v3 [48]	75.61	47.12	48.48	48.33	47.01
	MobileNet [49]	76.72	50.41	49.90	50.28	47.58
	VGG-16 [50]	78.77	51.82	50.39	51.08	48.69
	ResNet-50 [51]	80.27	52.44	51.50	52.94	49.75
	AlexNet [52]	81.34	53.41	53.37	54.08	51.28
	<i>ScarNet</i>	<b>81.89</b>	<b>54.02</b>	<b>53.46</b>	<b>54.79</b>	<b>53.60</b>
With (augmentation)	Inception-v3 [48]	87.43	76.52	76.11	75.05	73.23
	MobileNet [49]	88.21	77.56	76.68	77.31	73.80
	VGG-16 [50]	89.31	80.65	77.03	78.97	74.14
	ResNet-50 [51]	89.88	79.67	77.5	79.36	74.01
	AlexNet [52]	91.47	78.63	78.84	82.23	74.81
	<i>ScarNet</i>	<b>92.53</b>	<b>81.33</b>	<b>82.24</b>	<b>95.38</b>	<b>76.70</b>

**TABLE 9.** Comparison between the proposed ScarNet and five pre-trained models in terms of network parameters and accuracy.

Parameters	Inception-v3 [48]	MobileNet [49]	ResNet-50 [51]	AlexNet [52]	VGG-16 [50]	<i>ScarNet</i>
Model Size	92MB	49MB	98MB	294MB	528MB	<b>18MB</b>
Training Parameters	23.9M	4.2M	25.6M	61M	138M	<b>0.895M</b>
No. of Layers	48	30	177	25	41	<b>19</b>
Epochs	200	200	200	200	200	<b>50</b>
Running-time (s)	2535	2262	1785	1092	2685	<b>217</b>
Accuracy	87.43%	88.21%	89.88%	91.47%	89.31%	<b>92.53%</b>

the effectiveness and efficiency of our system in automatic acne scar classification.

**H. FAILURE CASES**

A graphical representation of acne scar classification based on our ScarNet is illustrated in Fig. 8. Observing the correctly classified cases, our model can successfully categorize the acne scars into five classes with a high score difference. Despite the high-performance accuracy of our system, there

are also a few misclassification cases, as demonstrated in the second row of Fig. 8 (actual and wrongly predicted labels are represented with blue and red colors, respectively). However, comparing the confidence score, ScarNet classifies the acne scars wrongly, mostly with a slight difference in scores. Drawing inferences from deeply analyzing the misclassified acne images, the proposed system mostly challenges classifying the images with shadows, highly bright illumination, poor clarity, or low image quality.

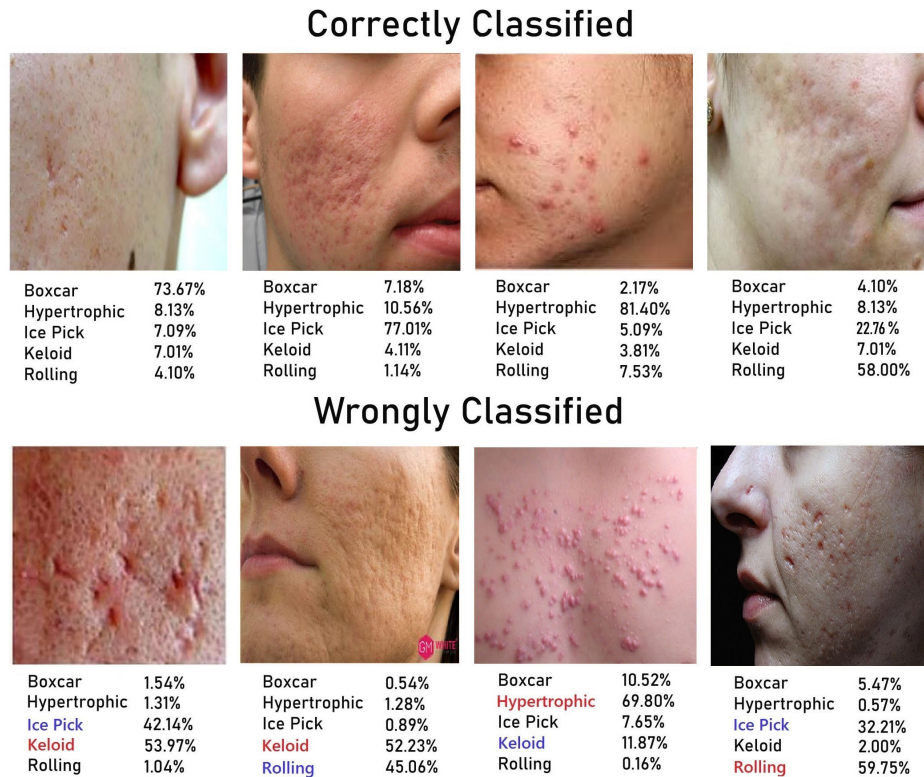


**FIGURE 8.** Graphical representation of acne scar classification. The top row is the correctly classified cases. The bottom row is the samples of wrongly classified images (blue and red colors indicate the actual and incorrectly predicted classes, respectively).

Misclassification also occurs when there are different acne scars within small skin regions simultaneously (e.g., fourth example in the misclassification cases).

### VI. CONCLUSION AND FUTURE WORKS

This paper presented an automated end-to-end CNN-based network for acne scar classification. An acne scar dataset was developed by capturing and collecting 250 images in 5 classes. These images were resized, and their quality was improved by designing a pre-processing module. The number of images was increased by applying five different augmentation techniques, which prevented the model from overfitting, increased its performance, and made it more robust. A novel deep CNN-based model was proposed to extract the feature maps from these images based on four convolution blocks and then classify them into five classes using fully connected and softmax layers. The performance of this system was investigated for different dataset splitting scenarios, number of epochs, and batch sizes. In this method, the influence of the augmentation was also analyzed. The feasibility and competitive performance of the proposed ScarNet was proved by conducting an extensive comparison with four conventional ML-based classifiers and five pre-trained models. Our system could accurately classify the acne scars with minimized computational cost compared to the other pre-trained models by adjusting the optimizer,

loss function, activation functions, filter and kernel sizes, regularization methods, and batch size. Experimental results demonstrated that the accuracy of our model is increased by 1.06%, 2.65%, 3.22%, 4.32%, and 5.1% compared to AlexNet, ResNet-50, VGG-16, MobileNet, and Inception-v3, respectively, without compromising the computational cost. As our future research work, we plan to extend our proposed acne scar dataset with more images and more classes for detecting the depth (shallow or deep) of some types of acne scars. Additionally, we will provide an automated system to segment and annotate different types of acne scars that appear in a close adjacent to each other on a small skin region.

### REFERENCES

- [1] G. Fabbrocini, M. Annunziata, V. D’arco, V. De Vita, G. Lodi, M. Mauriello, F. Pastore, and G. Monfrecola, “Acne scars: Pathogenesis, classification and treatment,” *Dermatol. Res. Pract.*, vol. 2010, Dec. 2010, Art. no. 893080.
- [2] J. Koo, “The psychosocial impact of acne: Patients’ perceptions,” *J. Amer. Acad. Dermatol.*, vol. 32, no. 5, pp. S26–S30, May 1995.
- [3] B. Dreno and F. Poli, “Epidemiology of acne,” *Dermatology*, vol. 206, no. 1, pp. 7–10, 2003.
- [4] J. K. L. Tan and K. Bhate, “A global perspective on the epidemiology of acne,” *Brit. J. Dermatol.*, vol. 172, pp. 3–12, Jul. 2015.
- [5] S. Zahra Ghodsi, H. Orawa, and C. C. Zouboulis, “Prevalence, severity, and severity risk factors of acne in high school pupils: A community-based study,” *J. Investigative Dermatol.*, vol. 129, no. 9, pp. 2136–2141, Sep. 2009.

- [6] A. Börve. (2021). *How Long do You Have to Wait for a Dermatologist Appointment*. Accessed: Apr. 14, 2021. [Online]. Available: <https://www.firstderm.com/appointment-wait-time-see-dermatologist>
- [7] C. I. Jacob, J. S. Dover, and M. S. Kaminer, "Acne scarring: A classification system and review of treatment options," *J. Amer. Acad. Dermatol.*, vol. 45, no. 1, pp. 109–117, Jul. 2001.
- [8] A. Goodarzi, E. Behrang, M. Ghassemi, N. N. Nobari, A. Sadeghzadeh-Bazargan, and M. Roohaninasab, "Acne scar: a review of classification and treatment," *J. Crit. Rev.*, vol. 7, no. 5, pp. 815–823, 2020.
- [9] D. Fife, "Practical evaluation and management of atrophic acne scars: Tips for the general dermatologist," *J. Clin. Aesthetic Dermatol.*, vol. 4, no. 8, p. 50, 2011.
- [10] G. J. Goodman and J. A. Baron, "Postacne scarring—A quantitative global scarring grading system," *J. Cosmetic Dermatol.*, vol. 5, no. 1, pp. 48–52, Mar. 2006.
- [11] B. Dreno, A. Khammari, N. Orain, C. Noray, C. Merial-Kieny, S. Méry, and T. Nocera, "ECCA grading scale: An original validated acne scar grading scale for clinical practice in dermatology," *Dermatology*, vol. 214, no. 1, pp. 46–51, 2007.
- [12] P. K. Upadhyay and S. Chandra, "An improved bag of dense features for skin lesion recognition," *J. King Saud Univ.-Comput. Inf. Sci.*, Feb. 2019.
- [13] Z. Wu, S. Zhao, Y. Peng, X. He, X. Zhao, K. Huang, X. Wu, W. Fan, F. Li, and M. Chen, "Studies on different CNN algorithms for face skin disease classification based on clinical images," *IEEE Access*, vol. 7, pp. 66505–66511, 2019.
- [14] P. Tang, Q. Liang, X. Yan, S. Xiang, and D. Zhang, "GP-CNN-DTEL: Global-part CNN model with data-transformed ensemble learning for skin lesion classification," *IEEE J. Biomed. Health Informat.*, vol. 24, no. 10, pp. 2870–2882, Oct. 2020.
- [15] R. Patil and S. Bellary, "Machine learning approach in melanoma cancer stage detection," *J. King Saud Univ.-Comput. Inf. Sci.*, Sep. 2020.
- [16] M. Combalia, F. Hueto, S. Puig, J. Malvehy, and V. Vilaplana, "Uncertainty estimation in deep neural networks for dermoscopic image classification," in *Proc. IEEE/CVF Conf. Comput. Vis. Pattern Recognit. Workshops*, Oct. 2020, pp. 744–745.
- [17] Y. Liu, A. Jain, C. Eng, D. H. Way, K. Lee, P. Bui, K. Kanada, G. de Oliveira Marinho, J. Gallegos, S. Gabriele, and V. Gupta, "A deep learning system for differential diagnosis of skin diseases," *Nature Med.*, vol. 26, no. 6, pp. 900–908, 2020.
- [18] L.-F. Li, X. Wang, W.-J. Hu, N. N. Xiong, Y.-X. Du, and B.-S. Li, "Deep learning in skin disease image recognition: A review," *IEEE Access*, vol. 8, pp. 208264–208280, 2020.
- [19] B. Ahmad, M. Usama, C.-M. Huang, K. Hwang, M. S. Hossain, and G. Muhammad, "Discriminative feature learning for skin disease classification using deep convolutional neural network," *IEEE Access*, vol. 8, pp. 39025–39033, 2020.
- [20] I. Iqbal, M. Younus, K. Walyat, M. U. Kakar, and J. Ma, "Automated multi-class classification of skin lesions through deep convolutional neural network with dermoscopic images," *Comput. Med. Imag. Graph.*, vol. 88, Mar. 2021, Art. no. 101843.
- [21] R. Mohakud and R. Dash, "Designing a grey wolf optimization based hyper-parameter optimized convolutional neural network classifier for skin cancer detection," *J. King Saud Univ.-Comput. Inf. Sci.*, Jun. 2021.
- [22] R. Ramli, A. S. Malik, A. F. M. Hani, and F. B.-B. Yap, "Identification of acne lesions, scars and normal skin for acne vulgaris cases," in *Proc. Nat. Postgraduate Conf.*, Sep. 2011, pp. 1–4.
- [23] B. C. Dey, B. Nirmal, and R. R. Galigekere, "Automatic detection of acne scars: Preliminary results," in *Proc. IEEE Point-Care Healthcare Technol. (PHT)*, Jan. 2013, pp. 224–227.
- [24] N. Alamdari, K. Tavakolian, M. Alhashim, and R. Fazel-Rezai, "Detection and classification of acne lesions in acne patients: A mobile application," in *Proc. IEEE Int. Conf. Electro Inf. Technol. (EIT)*, May 2016, pp. 0739–0743.
- [25] X. Shen, J. Zhang, C. Yan, and H. Zhou, "An automatic diagnosis method of facial acne vulgaris based on convolutional neural network," *Sci. Rep.*, vol. 8, no. 1, Dec. 2018, Art. no. 5839.
- [26] M. S. Junayed, A. A. Jeny, S. T. Atik, N. Neehal, A. Karim, S. Azam, and B. Shanmugam, "AcneNet—A deep CNN based classification approach for acne classes," in *Proc. 12th Int. Conf. Inf. Commun. Technol. Syst. (ICTS)*, Jul. 2019, pp. 203–208.
- [27] A. Z. Hameed, W. K. Awad, N. A. Irsan, and A. S. Abdulbaqi, "Hybrid technique for skin pimples image detection and classification," *Int. J. Adv. Sci. Technol.*, vol. 29, no. 3, pp. 4102–4109, 2019.
- [28] X. Wu, N. Wen, J. Liang, Y.-K. Lai, D. She, M.-M. Cheng, and J. Yang, "Joint acne image grading and counting via label distribution learning," in *Proc. IEEE/CVF Int. Conf. Comput. Vis.*, Apr. 2019, pp. 10642–10651.
- [29] K. Rashataprucks, C. Chuangchatchavarn, S. Triukose, S. Nitinawarat, M. Pongpruthipan, and K. Piromsopa, "Acne detection with deep neural networks," in *Proc. 2nd Int. Conf. Image Process. Mach. Vis.*, Aug. 2020, pp. 53–56.
- [30] C. Y. Chang and H. Y. Liao, "Automatic facial spots and acnes detection system," *J. Cosmetics, Dermatol. Sci. Appl.*, vol. 3, no. 1, p. 28, 2013.
- [31] A. S. Malik, R. Ramli, A. F. M. Hani, Y. Salih, F. B.-B. Yap, and H. Nisar, "Digital assessment of facial acne vulgaris," in *Proc. IEEE Int. Instrum. Meas. Technol. Conf.*, May 2014, pp. 546–550.
- [32] M. Khongsuwan, S. Kiattisin, W. Wongseree, and A. Leelasantitham, "Counting number of points for acne vulgaris using UV fluorescence and image processing," in *Proc. 4th Biomed. Eng. Int. Conf.*, Jan. 2012, pp. 142–146.
- [33] F. S. Abas, B. Kaffenberger, J. Bikowski, and M. N. Gurcan, "Acne image analysis: Lesion localization and classification," *Proc. SPIE Med. Imag. Comput.-Aided Diagnosis*, vol. 9785, Oct. 2016, Art. no. 97850B.
- [34] N. Kittigul and B. Uyyanonvara, "Acne detection using speeded up robust features and quantification using K-Nearest neighbors algorithm," in *Proc. 6th Int. Conf. Bioinf. Biomed. Sci.*, Jun. 2017, pp. 168–171.
- [35] T. Zhao, H. Zhang, and J. Spoelstra, "A computer vision application for assessing facial acne severity from selfie images," 2019, *arXiv:1907.07901*.
- [36] C. Kulshrestha, P. Juyal, S. Sharma, and S. Juyal, "Machine learning algorithms based skin disease detection," *Int. J. Innov. Technol. Exploring Eng.*, vol. 9, pp. 4044–4049, May 2020.
- [37] M. S. Junayed, A. N. M. Sakib, N. Anjum, M. B. Islam, and A. A. Jeny, "EczemaNet: A deep CNN-based eczema diseases classification," in *Proc. IEEE 4th Int. Conf. Image Process., Appl. Syst. (IPAS)*, Dec. 2020, pp. 174–179.
- [38] G. J. Goodman, "Postacne scarring: A review of its pathophysiology and treatment," *Dermatol. Surg.*, vol. 26, no. 9, pp. 857–871, 2000.
- [39] L. A. Zaleski-Larsen, S. G. Fabi, T. McGraw, and M. Taylor, "Acne scar treatment: A multimodality approach tailored to scar type," *Dermatol. Surg.*, vol. 42, pp. S139–S149, 2016.
- [40] A. Skin. (2021). *Dermnet NZ*. Accessed: Oct. 15, 2020. [Online]. Available: <https://dermnetnz.org/>
- [41] K. He, J. Sun, and X. Tang, "Guided image filtering," *IEEE Trans. Pattern Anal. Mach. Intell.*, vol. 35, no. 6, pp. 1397–1409, Jun. 2013.
- [42] C. Tomasi and R. Manduchi, "Bilateral filtering for gray and color images," in *Proc. 6th Int. Conf. Comput. Vis.*, 1998, pp. 839–846.
- [43] P. J. Baldevbhai and R. Anand, "Color image segmentation for medical images using  $L^* a^* b^*$  color space," *IOSR J. Electron. Commun. Eng.*, vol. 1, no. 2, pp. 24–45, 2012.
- [44] M. S. Junayed, N. Anjum, A. Noman, and B. Islam, "A deep CNN model for skin cancer detection and classification," in *Proc. 29th Int. Conf. Central Eur. Comput. Graph., Vis. Comput. Vis. (WSCG)*, 2021, pp. 71–80.
- [45] F. Demir, A. Sengur, and V. Bajaj, "Convolutional neural networks based efficient approach for classification of lung diseases," *Health Inf. Sci. Syst.*, vol. 8, no. 1, pp. 1–8, Dec. 2020.
- [46] S. Bagchi, A. Banerjee, and D. R. Bathula, "Learning a meta-ensemble technique for skin lesion classification and novel class detection," in *Proc. IEEE/CVF Conf. Comput. Vis. Pattern Recognit. Workshops (CVPRW)*, Jun. 2020, pp. 746–747.
- [47] I. Fantini, C. Yasuda, M. Bento, L. Rittner, F. Cendes, and R. Lotufo, "Automatic mr image quality evaluation using a deep CNN: A reference-free method to rate motion artifacts in neuroimaging," *Comput. Med. Imag. Graph.*, vol. 90, Oct. 2021, Art. no. 101897.
- [48] C. Szegedy, V. Vanhoucke, S. Ioffe, J. Shlens, and Z. Wojna, "Rethinking the inception architecture for computer vision," in *Proc. Conf. Comput. Vis. Pattern Recognit.*, 2016, pp. 2818–2826.
- [49] A. G. Howard, M. Zhu, B. Chen, D. Kalenichenko, W. Wang, T. Weyand, M. Andreetto, and H. Adam, "MobileNets: Efficient convolutional neural networks for mobile vision applications," 2017, *arXiv:1704.04861*.
- [50] K. Simonyan and A. Zisserman, "Very deep convolutional networks for large-scale image recognition," 2014, *arXiv:1409.1556*.
- [51] K. He, X. Zhang, S. Ren, and J. Sun, "Deep residual learning for image recognition," in *Proc. IEEE Conf. Comput. Vis. Pattern Recognit.*, Oct. 2016, pp. 770–778.
- [52] A. Krizhevsky, I. Sutskever, and G. E. Hinton, "ImageNet classification with deep convolutional neural networks," *Commun. ACM*, vol. 60, no. 2, pp. 84–90, Jun. 2012.



**MASUM SHAH JUNAYED** (Member, IEEE) received the bachelor's degree in computer science and engineering from Daffodil International University, in 2019. He is currently pursuing the master's degree with the Department of Computer Engineering, Bahçeşehir University (BAU), Istanbul, Turkey. Currently, he is a Graduate Research Assistant at the Computer Vision Laboratory under TUBITAK 2232 Project. Previously, he worked as a Research Assistant at the Gradient Lab for AI

Research (GLAIR). He is a member of the Machine Intelligence Research Laboratory (MIR Lab) and the Founder and the Director of the Vision Research Lab of AI (VRLAI). He has published several peer-reviewed conferences and journal articles. His research interests include computer vision, machine learning, image and video processing, and medical image analysis.



**MD BAHARUL ISLAM** (Senior Member, IEEE) received the B.Sc. degree in computer science and engineering from RUET, Bangladesh, the M.Sc. degree in digital media from Nanyang Technological University, Singapore, and the Ph.D. degree in computer science from Multimedia University, Malaysia. Before becoming a Faculty Member, he was a Postdoctoral Research Fellow at the AI and Augmented Vision Laboratory, Miller School of Medicine, University of Miami, USA.

He has more than 15 years of working experience in teaching and cutting-edge research in image processing and computer vision. He has authored/coauthored more than 40 international peer-reviewed research papers, including journal articles, conference proceedings, books, and book chapters. His current research interests include 3D processing and AR/VR-based vision rehabilitation. He secured several gold medals and best paper awards from national and international scientific and technological competitions and conferences. His Ph.D. thesis was selected for the best research work by the IEEE SPS Research Excellence Award, in 2018. He was awarded the International Fellowship and Grant for Outstanding Young Researchers from the Scientific and Technological Research Council of Turkey (TUBITAK), in 2019.



**AFSANA AHSAN JENY** received the bachelor's degree in computer science and engineering from Daffodil International University, in 2019. She is currently pursuing the master's degree with the Department of Computer Engineering, Bahçeşehir University (BAU), Istanbul, Turkey. Currently, she is a Graduate Research Assistant at BAU Computer Vision Laboratory under TUBITAK 2232 Project. Previously, she worked as a Research Assistant at Gradient Lab for AI

Research (GLAIR). She is a member of the Machine Intelligence Research Laboratory (MIR Lab). She has published several peer-reviewed conferences and journal articles. Her research interests include computer vision, machine learning, video processing, medical image processing, and artificial intelligence.



**AREZOO SADEGHZADEH** received the B.S. degree in electrical engineering from Azarbaijan Shahid Madani University, Tabriz, Iran, in 2014, and the M.S. degree in electrical engineering (telecommunication) from the Sahand University of Technology, Tabriz, in 2016. She is currently pursuing the Ph.D. degree with the Computer Engineering Department, Bahçeşehir University (BAU), Istanbul, Turkey. She is currently working on sign language recognition and

translation and visual field map assessment at the Computer Vision Laboratory, BAU. Previously, she worked as a Lecturer with the Computer Engineering Department, University College of Nabi Akram, Tabriz. Her research interests include artificial intelligence, image and video processing, computer vision, and machine learning.



**TOPU BISWAS** (Member, IEEE) received the B.Sc. degree in electrical and electronic from the Pabna University of Science and Technology (PUST) and the Master of Engineering Science (M.Eng.Sc.) degree from Multimedia University (MMU). After completing his bachelor's degree, he achieved a research scholarship to pursue his master's degree in MMU, which is funded by the Ministry of Science and Technology (MOSTI), Malaysia. His research interests include

developing different machine learning and artificial intelligence-based systems to advance healthcare through the lens of equity inclusion. The research project "Automated Diagnosis and Prognosis of Chronic Wounds for e-Health Applications (part of his master's degree) have been awarded eight national and international awards, including the Gold Medal and "the Best of the Best Award (within 247 Projects)." Apart from his study, he also held different leadership positions. He was the Founding Chair of IEEE PUST Student Branch and Elected President for MMU Postgraduates Society (2019/2020) which represents the interests of all MMU postgraduate students of the two campuses and eight faculties at MMU.



**A. F. M. SHAHEN SHAH** (Senior Member, IEEE) received the B.Sc. degree in electronics and telecommunication engineering from Daffodil International University, Dhaka, Bangladesh, in 2009, the M.Sc. degree in information technology from the University of Dhaka, Dhaka, in 2011, and the Ph.D. degree in electronics and communication engineering from Yildiz Technical University, Istanbul, Turkey, in 2020. He worked as an Assistant Professor with the Department

of Electrical and Electronics Engineering, Istanbul Gelisim University, Istanbul, from 2020 to 2021. He also worked in industry for ten years, where he served as a higher management position. Since 2021, he has been working as an Assistant Professor with the Department of Electronics and Communication Engineering, Yildiz Technical University. He has authored a book. He has published a good number of research papers in international conferences and journals. His current research interests include wireless communication, artificial intelligence, 6G, blockchain, and cross-layer design. He is a Life Member of the Institution of Engineers, Bangladesh (IEB).

...